

Final Draft
of the original manuscript:

Rao, D.; Huber, K.; Heerens, J.; dos Santos, J.F.; Huber, N.:
**Asymmetric mechanical properties and tensile behaviour
prediction of aluminium alloy 5083 friction stir welding joints**
In: Materials Science and Engineering A (2012) Elsevier

DOI: 10.1016/j.msea.2012.12.014

Asymmetric mechanical properties and tensile behaviour prediction of aluminium alloy 5083 friction stir welding joints

D. Rao^{1*}, K. Huber², J. Heerens², J. F. dos Santos², N. Huber²

1, Dept. of Mechanical Engineering, Shanghai Jiao Tong University, China
2, Institute of Materials Research, Helmholtz-Zentrum Geesthacht, Germany

ABSTRACT

The asymmetric material flow, severe plastic deformation and thermal cycle imposed on the base material during friction stir welding (FSW) result in unique microstructural development, which causes a gradient in local mechanical properties in the weld region. Micro-tensile and indentation testing were applied to determine the local mechanical properties in a friction stir welded joint. The local stress-strain curves exhibited a drastic change at the advancing side (AS) due to a steep gradient of mechanical properties. Finite Element Model (FEM) predictions of the tensile performance of the welded joints, based on the local mechanical properties measured by micro-tensile testing, were in very good agreement with the macro-tensile test data.

Keywords: Friction stir welding (FSW); Aluminium alloy; Mechanical properties testing; Microstructure; Finite element model (FEM)

1. Introduction

In conventional welding processes that employ inert or active shielding gas, e.g., Gas Metal Arc Welding (GMAW), the microstructural and mechanical properties of both sides of a weld are symmetric, as observed in the case of a butt joint. This symmetry exists because the temperature field is identically mirrored when similar metals are welded; the temperature field is the main factor that affects the microstructural and mechanical properties of the heat affected zone (HAZ). Friction stir welding (FSW) is a solid-state welding method, which was developed less than 20 years ago. During FSW, the base metal is severely deformed and heated by a rotating tool with a pin. The pin stirs the plasticised material, and the weld joint is formed by the plastic deformation of the softened metal. The simultaneous rotation and transverse motion of the pin creates asymmetry between the two sides of the weld. The pin rotation and welding direction are the same on the advancing side (AS) and are opposite on the retreating side (RS) of the weld. The asymmetry of the welded joint is a unique characteristic of the FSW method.

The micro- and macrostructure of aluminium alloy FSW joints have been investigated by many researchers [1-4]. Traditional tensile specimens are often used to describe the mechanical properties of FSW joints [3, 5, 6, 7]. The specimens are usually machined perpendicular to the weld line, and each specimen covers the base metal, the

* Delin Rao, corresponding author, email: raode@sjtu.edu.cn Tel: 86-21-34206560 Fax: 86-21-34205182

HAZ, the thermo-mechanically affected zone (TMAZ) and the stir zone (SZ) regions. Therefore, the macro-tensile testing results describe the complex structural response that results from the interplay among all of these regions. Thus, it is hard to investigate the asymmetric mechanical properties of a FSW joint with conventional macro-tensile specimens. Some studies have examined the microstructural asymmetry of FSW joints [5, 8, 9]. Due to their dissimilar heat inputs, the temperature fields measured on the RS and the AS are different [10]. However, as the local mechanical properties across the FSW joint are not easily measured, the asymmetry at the RS and the AS, especially the mechanical properties of the two sides, have not been fully investigated, which is the main subject of this work. Although the local strain in a FSW joint can be measured using the electronic speckle pattern interferometer technique [11], the local stress distribution due to the inhomogeneous deformation of the macro tensile specimen must be measured to determine its local mechanical properties.

The 5083 aluminium alloy is a light metal alloy that has a high degree of corrosion resistance combined with an excellent balance of mechanical properties. Therefore, it is widely used as a structural material in transportation applications. In this study, a micro-tensile method was applied to evaluate the spatial dependence of the mechanical properties of an Al 5083 FSW joint in detail. Stress-strain data from indentation experiments were taken from previous work for comparison [12]. Residual stress will not significantly affect the micro-tensile results considering the size of the micro-tensile specimens and the manufacturing method used to produce them [12]. The asymmetry of microstructural and mechanical properties between the AS and the RS of the Al 5083 FSW joint were investigated and discussed. A Finite Element Model (FEM) was then carried out to evaluate its predictive capabilities for each approach used to measure the local mechanical properties.

2. Experimental procedures

2.1 Production of welded samples

The base material consisted of a cold rolled H-temper Al 5083 aluminium alloy (Al-4.5Mg-0.6Mn) plate that measured 120 mm in width, 400 mm in length, and 3 mm in thickness. Friction stir butt welds were made using a tool with a 12 mm concave shoulder and a 5 mm conical pin. The welds were produced with a rotational speed, welding speed and axial force of 1800 RPM, 1000 mm/min and 9.5 kN, respectively.

Two samples were cut perpendicular to the welding direction. One of these samples was used for metallographic analysis and hardness testing. The specimens were mounted, polished and etched for 75~90 s in Barker's reagent. The etched surface of the sample containing the FSW joint was observed in an optical microscope, and the hardness testing was conducted along the transverse section of the welded joint in a Shimadzu HMV-2000.

2.2 Micro- and macro-tensile testing

The local changes in the mechanical properties across the welded joint were determined by micro-tensile testing. To obtain micro-tensile specimens, a rectangular section of the welded plate was sliced into many specimens using spark erosion. The dimensions and orientation of the micro-tensile specimen are illustrated schematically in Figure 1. 51 micro-tensile specimens were produced that spanned approximately 15 mm on each side of the weld centreline. Micro-tensile testing was carried out on a Zwick/Z005 tensile machine with a strain rate of 0.2 mm/min.

The micro-tensile specimens were extracted from the base material, the HAZ, the TMAZ and the SZ. The AS and the RS of the joint were sampled separately (Figure 1, bottom). The thickness of each micro-tensile specimen was approximately 0.4 mm. The width in the gauge section and the total length were approximately 1.4 mm and 25 mm, respectively. The micro-tensile specimens were tested using a specially designed fixture that ensured the correct application of the load and prevented secondary bending and other unwanted movement of the specimens (Figure 2). Before testing, the surfaces of the specimens were marked with white lines to allow for the measurement of strain using a laser beam scanning apparatus.

The macro-tensile testing was carried out on a conventional tensile test machine. The thickness of the specimen was 3 mm (the same as the original thickness of the weld plate). The specimen was cut from a weld plate that was 25 mm in width and 240 mm in length. The FSW line was placed on the middle of the specimen, perpendicular to the tensile loading direction (Figure 1, top).

2.3 Indentation test

The indentation testing was performed using a Zwick test machine ZHU 0.2/Z2.5 that was equipped with a hardness measurement head and a fully automated X/Y table. A diamond Rockwell indenter with a spherical tip of radius $R = 200 \mu\text{m}$ was installed and used for all indentation tests. All tests were performed under load-controlled conditions in an air-conditioned room at a temperature of 21 °C.

The indentation approach used in this work has been published in detail in [12] and will be summarised here. The analysis of the indentation data provides a stress-strain curve for each individual indent, similar to a micro-tensile analysis. Indentation testing and Artificial Neural Network (ANN) analysis require only a well-polished surface, and they can be considered almost non-destructive compared to micro-tensile testing. With a spherical indenter, a hemispherical volume of material is tested locally under compression loading, producing a large hydrostatic pressure. Therefore, material failure does not occur; elongation to failure cannot be determined from an indentation test.

However, the technique allows local yielding and work hardening behaviour to be mapped for a cross-section. In the present case, a row of indentation tests were performed on the weld cross-section along the centreline (Figure 3). Because of the large strains that occurred during this test, it was more sensitive to the yield stress behaviour around a 10% plastic strain. It showed larger uncertainties below, above and, in particular, near the yield point [13-15]. Thus, this approach is favourable for studies that investigate the deformation behaviour of specimens under significant plastic deformation. The following section will elaborate on this point in more detail, particularly with regard to the prediction of the performance of the macro-tensile specimens.

3. Results and discussion

3.1. Asymmetry of microstructure

The asymmetry of the macrostructure of the FSW joint was significant. Figure 3 shows distinct differences between the AS and the RS. The microstructure variation from the SZ to the TMAZ was more drastic at the AS than at the RS. An asymmetric “onion ring” structure was also found in the SZ [16]. The ring structure was very clear in the SZ close to the AS, but it was not especially well-defined in the SZ close to the RS. Even at the AS, the distance between rings varied. It decreased when progressing from the centre towards the periphery. This finding was in agreement with those of

previous researchers [16]. The mechanism of formation of the “onion ring” structure is still not completely clear, but some possible explanations can be found in the literature [17, 18]. Figure 3 shows that the border between the TMAZ and the SZ at the AS was very abrupt; such behaviour is typically observed in FSW [1, 4, 11], but the border is much more diffuse at the RS. More detail can be seen in Figure 4, which shows the microstructure of the SZ and the TMAZ.

Figure 4 (a) depicts the TMAZ microstructure at the AS. At the TMAZ, the coarse grains were severely deformed by the plastic flow created by the stir action of the rotating pin. The orientation of the grains in this region was almost perpendicular to the rolling direction. A discernible border was visible between the SZ and the TMAZ. Figure 4 (b) shows the TMAZ microstructure of the RS. The equiaxed grains of the SZ can be observed at the right side of the figure, and the TMAZ grains can be observed at the left side. At the RS, it was more difficult to define a transition line between the SZ and the TMAZ grains.

3.2. Hardness profiles

Al 5083 is a non-heat-treatable Al–Mg alloy, and its strength is primarily due to a high solute concentration and the associated strain hardening [11, 19]. During the welding process, the high strain rate deformation and high temperatures can cause substantial microstructural variations that affect the hardness profile of the material.

Vickers hardness values were measured along the transverse section of the Al 5083 joint (Figure 5). The base material had a higher hardness (average hardness approximately 95 HV) than the weld (the SZ, the TMAZ and the HAZ); the weld had an average hardness of approximately 85 HV. The hardness profile was asymmetric for the AS and the RS. At the AS, moving inwards from the base material to the HAZ, the hardness began to drop sharply approximately 7 mm from the weld centre; the hardness reached a minimum of approximately 80 HV, 4 mm from the weld centre. The gradient of hardness at the AS of the HAZ was approximately 5 HV/mm. At the RS and moving inwards, the hardness fell more gradually beginning approximately 10 mm from the weld centre and reached a minimum of approximately 85 HV. The gradient of the hardness at the RS of the HAZ was approximately 2 HV/mm, which was only half of that at the AS. Moreover, Figure 5 shows that the width of the HAZ at the AS was smaller than that at the RS. This occurs because the temperature profile around the weld was asymmetric, and the thermal field was wider at the RS [20]. From analysing the hardness profile and comparing it to the observed microstructure (Figure 3), it is evident that the minimum hardness region was located at the HAZ, not at the SZ. The resulting hardness profile demonstrated an asymmetric U shape.

3.3 Micro-tensile testing

Serrated yielding is a common phenomenon observed during the tensile testing of 5xxx aluminium alloys [21]. During a tensile test, serrated flow occurs after the yield point. Then, the stress drops, and the serration intensity increases with strain [22]. Serrated yielding was observed in all micro-tensile curves for the 5083 aluminium alloy used in this study. For the sake of clarity, the data points on the engineering stress-strain curves describe the average strain amplitude over the serration cycle after the yield point.

The engineering stress-strain curves of the micro-tensile specimens at the AS are illustrated in Figure 6. The solid circles show the behaviour of the Al 5083 base material, and they each represent the average value obtained from the measurements of ten specimens. From the base material to the HAZ, the yield strength of the specimen

dropped gradually, while the fracture strain increased. A large gradient in yield strength was found 6.6 mm from the weld centre. However, the stress-strain curves showed a dramatic drop 6.6 mm to 6.0 mm from the weld centre. The maximum fracture strain was found 6.0 mm from the weld centreline. The variation of the yield stress in the micro-tensile sample qualitatively matched the measured hardness profile shown in Figure 5.

Figure 7 shows the engineering stress-strain curves at the RS of the welded joint. The strength of the material decreased from the base material to the HAZ, whereas the ductility increased at the RS. The engineering stress-strain curves and the hardness data revealed an analogous trend at the AS, but the gradients in mechanical properties at the RS were slightly smaller. There was also a steep gradient at the RS of the HAZ, approximately 6.0 mm from the weld centreline. For comparative purposes, the yield stress and the true stress of the 51 test specimens at a given true strain of 2% and 4% were plotted across the welded joint in Figure 8. The average yield stress of the base material was approximately 215 MPa. As the HAZ was approached, the strength dropped drastically and then stabilised in the SZ. The average yield stress of the SZ was approximately 160 MPa, 25% lower than that of the base material. This strength decrease is due to recovery and recrystallisation in the weld zone. The finer grain size of the SZ indicated that dynamic recovery and recrystallisation occurred, which reduced the dislocation density in this region [23, 24]. As already indicated in the analysis of the hardness profiles, the yield stress behaviour was asymmetric for both sides of the weld. At the AS, the drop in the yield stress curve spanned 1.5 mm (-8.5 mm to -6 mm); at the RS, it spanned more than 3 mm. Thus, the yield strength gradient present at the AS was more than twice that present at the RS. When compared to the hardness distribution (Figure 5), the true stress profile revealed a closer agreement between the tensile strength and hardness results (Figure 8). However, because a larger volume was tested by the micro-tensile specimen, the scatter in strength is much lower.

In addition to the difference in strength between the AS and RS, the ductility of both sides also differed. Figure 9 shows the fracture strain of the micro-tensile specimens across the welded joint. The fracture strain of the base material was approximately 16%. There was a lot of scatter in the data, but the general trend in the results suggested that the fracture strain was over 20% close to the SZ. At the AS (from specimen No. 20 to No. 21, see Figure 8), the fracture strain also increased more rapidly than at the RS. The high fracture strains were due to recovery and recrystallisation, which occurred to different degrees in the weld zones and resulted in a reduction in yield strength and an increase in strain hardening capacity in the tensile tests compared with the original work hardened plate. These factors allowed a larger stable elongation before necking in the micro-tensile tests. The ductility increased not only in the fine-grained SZ but also in the HAZ. As the HAZ retained the same grain structure as the base material without significant plastic strain, it can be assumed that recovery is responsible for the increase in ductility [25].

3.4 Macro-tensile tests

The behaviour of the FSW specimens during macro-tensile testing follows the basic principles of mechanics. In defect-free joints without a geometric surface notch, plastic strain becomes concentrated, and failure always takes place at the weakest region of the microstructure. In FSW, with a given Al alloy family, failure can also occur in the TMAZ when a weld defect exists, depending on the tool geometry and on the process parameters [26].

Two macro-tensile specimens (A3, A4) were cut from the same plate as the micro-tensile specimens (Figure 1). An overview of the failure of one of these specimens is shown in Figure 10 (a). As stated in section 3.2, the softening in the HAZ in the Al 5083 FSW joint took place during FSW. The HAZ exhibited the lowest hardness and strength; as a result, the fracture occurred in the HAZ [27]. Figure 10 (a) shows that failure occurred in the HAZ at the RS under tensile loading. Figure 10 (b) shows a cross-section through the failed weld. It can be observed that the fracture path was approximately 4 mm from the weld centre, which means it was in the HAZ or between the TMAZ and the HAZ. The profile of the crack path looks identical to the SZ profile at the RS, but the presence of defects or a geometric surface notch may cause deviation from the expected behaviour. Such a deviation did occur for the welded joint that was investigated in this study. Figure 10 (c) provides more detail of the weld surface region. A weld flaw was observed in this region, which was a remnant of an oxide array. This type of flaw is referred to as a “kissing bond”, and it is known to induce cracking [28]. Thus, the failure path changed along the flaw in this region. The failure path of the macro-tensile specimen was determined by the presence of this defect (i.e., weld flaw), and it followed the most energetically favourable path (i.e., the zone with the weakest microstructure).

3.5 Prediction of the macro-tensile behaviour

To predict the macroscopic force-displacement behaviour of the macro-tensile specimens, a 3D FEM with the same dimensions as the macro-tensile specimen was generated. The FEM mesh consisted of 24,159 quadrilateral elements (C3D8) with 3 elements through the thickness (z) and 54 elements normal to the loading direction (y) within the gage length. The resulting element dimensions were approximately 1 mm and 0.5 mm in the z - and y -direction, respectively. The discretisation in loading direction was 2 mm (Figure 11). Nonlinear isotropic hardening and large deformation theory was used. The nonlinear stress-strain behaviour was defined in the ABAQUS input file using piecewise linear segments for the true stress-true plastic strain behaviour as provided by the ANN prediction for a given position y . The mapping of the material behaviour from the 51 micro-tensile curves to the FEM was performed using an ANN. It helped to smooth the experimental curves and interpolate the material behaviour to the position of the elements in the model at a resolution of 1 mm (i.e., two neighbouring elements in the loading direction shared the same material law).

The experimental global force-displacement behaviour and the FEM predictions are compared in Figure 12. With regard to the experimental data, it can be observed that the specimen A3 fractured early. Assuming a strain gauge of $L_0 = 50$ mm, the fracture elongation of 0.44 mm corresponds to approximately a 0.9 % strain. Specimen A4 showed a higher value of 1.8 mm (3.6 % strain) with some instabilities occurring between 0.9 mm elongation and final fracture. The instabilities indicated the formation of a crack, which extended discontinuously with increasing load. This observation matched the zigzag shape of the crack path, as shown in Figure 10.

Figure 12 shows the experimental force-displacement curve from the macro-tensile test together with the obtained FEM predictions based on micro-tensile and indentation experiments. It can be observed that the predictions based on the micro-tensile experiments fit the measured force-displacement curve perfectly well. However, when the local properties were measured by micro-indentation, the yield stress was overestimated by approximately 2 kN (30 MPa). This discrepancy resulted from the limited sensitivity to the stress-strain behaviour around the yield point; this technique was more robust with approximately 8-12% plastic strain, as discussed in section 2.3.

As a consequence, when using stress-strain data from the indentation analysis, the predicted macro-tensile force-displacement curve approached both the experimental curve as well as the prediction based on the micro-tensile data after approximately 0.5 mm elongation, when the initial curvature around the yield point had been passed.

4. Conclusions

An investigation of the asymmetric distribution of microstructure and local mechanical properties in an Al 5083 FSW butt joint was carried out. It was found that the change in hardness occurred more rapidly at the AS than at the RS. The hardness decreased sharply from the HAZ to the SZ at the AS; at the RS, this gradient was small. The hardness profile demonstrated an asymmetric U shape with a global minimum in the HAZ of the AS.

Micro-tensile testing showed that, similar to the hardness distribution, the engineering stress-strain curves were also asymmetric at both sides of the weld. The yield strength gradient in the HAZ at the AS was more than twice that at the RS. The distribution of the fracture strain showed that strong recovery occurs at both the AS and the RS of the FSW joint, and the fracture strain is very sensitive to the position of the specimen on the AS.

Macro-tensile tests showed that the Al 5083 FSW joint fractured at the RS of the HAZ. Although the strength was lower at the AS, the crack initiated at the RS because of the presence of a root flaw. The FEM predictions of the macro-tensile strength were in good agreement for elongations above 0.5 mm when the micro-tensile test data were used. Below this value, the predictions matched the macro-tensile experiments perfectly well, while the prediction based on indentation data overpredicted the specimen strength by approximately 2 kN (30 MPa). However, it can be concluded that indentation based stress-strain curves, which can be collected over the cross-section of a specimen, are sufficiently accurate for predicting the specimen strength at plastic strains above 1%. If the goal is the prediction of the performance of the joint well above 0.5 mm elongation, simple indentation tests provide comparable values to those obtained from time consuming micro-tensile tests.

Acknowledgements

The authors would like to thank Ms. P. Fischer (HZG, Germany) for assistance with the optical microscopy and Dr. D. Hellmann (HZG, Germany) for assistance with the SEM images.

References

- [1] Y.J. Kwon, I. Shigematsu, N. Saito, *Scripta Materialia*. 49(2003)785-789
- [2] M. Amirizad, A.H. Kokabi, M. Abbasi Gharacheh, R. Sarrafi, B. Shalchi, M. Azizieh, *Materials Letters*. 60(2006) 565-568
- [3] Shusheng Di, Xinqi Yang, Guohong Luan, Bo Jian, *Materials Science and Eng. A*. 435-436(2006) 389-395
- [4] Hanadi G. Salem, *Scripta Materialia*. 49(2003)1103-1110
- [5] T.S. Srivatsan, Satish Vasudevan, Lisa Park, *Materials Science and Eng. A*. 466(2007) 235-245
- [6] Caizhi Zhou, Xinqi Yang, Guohong Luan, *Scripta Materialia*. 54(2006)1515-1520
- [7] H. Jamshidi Aval, S. Serajzadeh, A.H. Kokabi, *Materials Science and Eng. A*. 528 (2011) 8071-8083

- [8] A. Barcellona, G. Buffa, L. Fratini, D. Palmeri, *Journal of Materials Processing Technology*. 177(2006)340-343
- [9] Tomotake Hirata, Taizo Oguri, Hideki Hagino, Tsutomu Tanaka, Sung Wook Chung, Yorinobu Takigawa, Kenji Higashi, *Materials Science and Eng. A*. 456(2007)344-349
- [10] L. Commin, M. Dumont, J.-E. Masse, L. Barrallier, *Acta Materialia*. 57(2009)326-334
- [11] M. Peel, A. Steuwer, M. Preuss, P.J. Withers, *Acta Materialia*. 51(2003) 4791-4801
- [12] D.Rao, J. Heerens, G. Alves Pinheiro, J.F. dos Santos, N. Huber, *Materials Science and Eng. A* 527(2010) 5018-5025
- [13] E. Tyulyukovskiy, N. Huber, *J. Mater. Res.* 21(2006)664-676
- [14] D. Klötzer, C. Ullner, E. Tyulyukovskiy, N. Huber, *J. Mater. Res.* 21(2006) 677-684
- [15] J. Heerens, F. Mubarok, N. Huber, *J. Mater. Res.* 24(2009)907-917
- [16] K.N.Krishnan, *Materials Science and Eng. A*. 327(2002)246-251
- [17] H.N.B. Schmidt, T.L.Dickerson, J.H.Hattel, *Acta Materials* 54(2006)1199-1209
- [18] Amir Abbas Zadpoor, Jos Sinke, Rinze Benedictus, Raph Pieters, *Materials Science and Eng. A* 494 (2008) 281-290
- [19] A. Steuwer, M.J. Peel, P.J. Withers, *Materials Science and Eng. A* 441 (2006) 187-196
- [20] R. Nandan, G.G. Roy, T.J. Lienert, T. Debroy, *Acta Materialia*. 55(2007)883-895
- [21] Hanging Zhu, A.K. Ghosh, K. Maruyama, *Materials Science and Eng. A* 419 (2006):115-121
- [22] G.R. Cui, Z.Y. Ma, S.X. Li, *Acta Materialia*. 57 (2009)5718-5729
- [23] Kwansoo Chung, Wonoh Lee, Daeyong Kim, Junehyung Kim, Kyung-Hwan Chung, Chongmin Kim, Kazutaka Okamoto, R.H.Wagoner, *International Journal of Solids and Structures*. 47 (2010) 1048-1062
- [24] T.R. McNelley, S. Swaminathan and J.Q. Su, *Scripta Materialia*. 58 (2008) 349-354
- [25] S.N. Patankar and Tan Ming Jen, *Scripta Materialia*. 38(1998)1255-1261
- [26] H.J. Zhang, H.J. Liu, L. Yu, *Materials and Design*. 32(2011) 4402-4407
- [27] S.R. Ren, Z.Y. Ma, L.Q. Chen, *Scripta Materialia*. 56 (2007) 69-72
- [28] Yutaka S. Sato, Hideaki Takauchi, Seung Hwan C. Park, Hiroyuki Kokawa, *Materials Science and Eng. A* 405(2005) 333-338

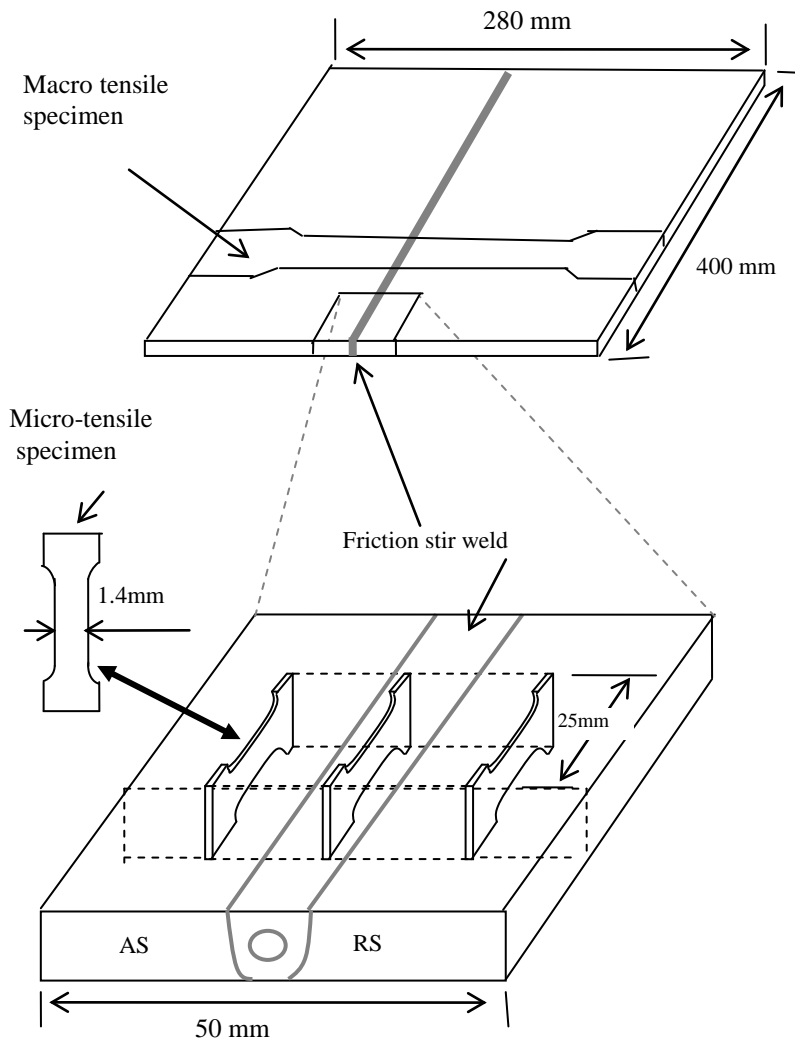


Figure 1 Position and orientation of micro-tensile specimens.

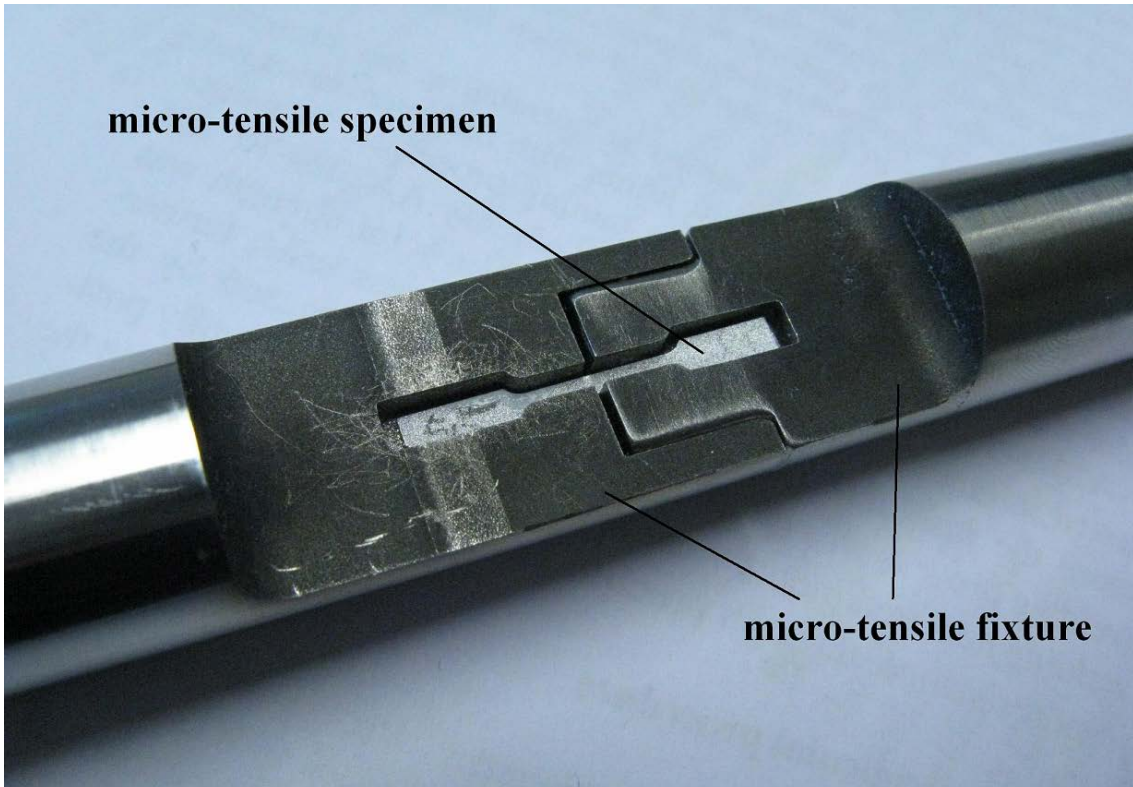
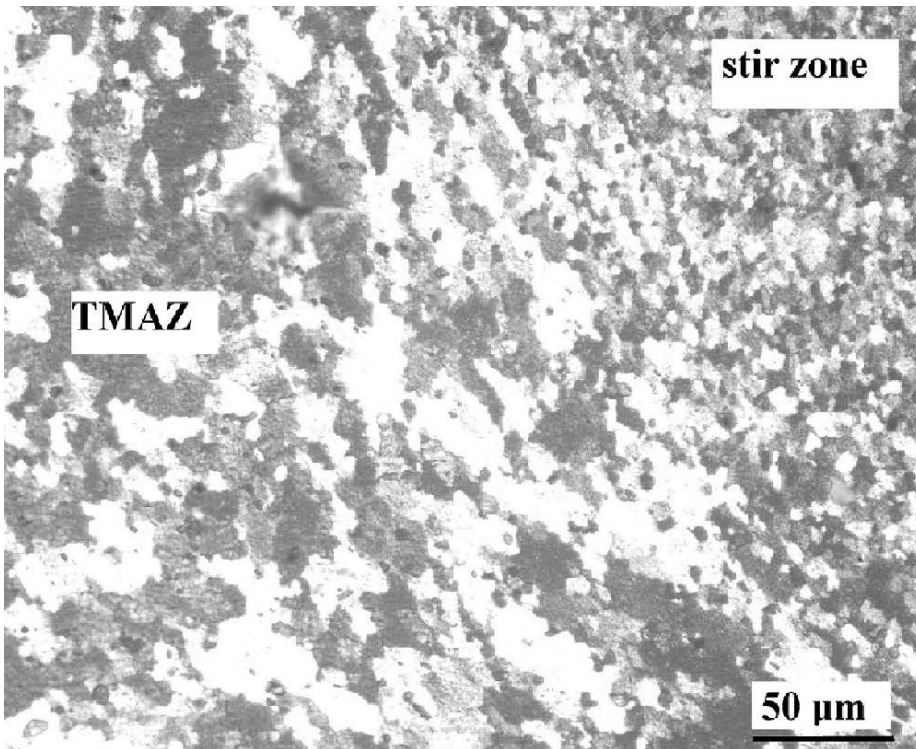


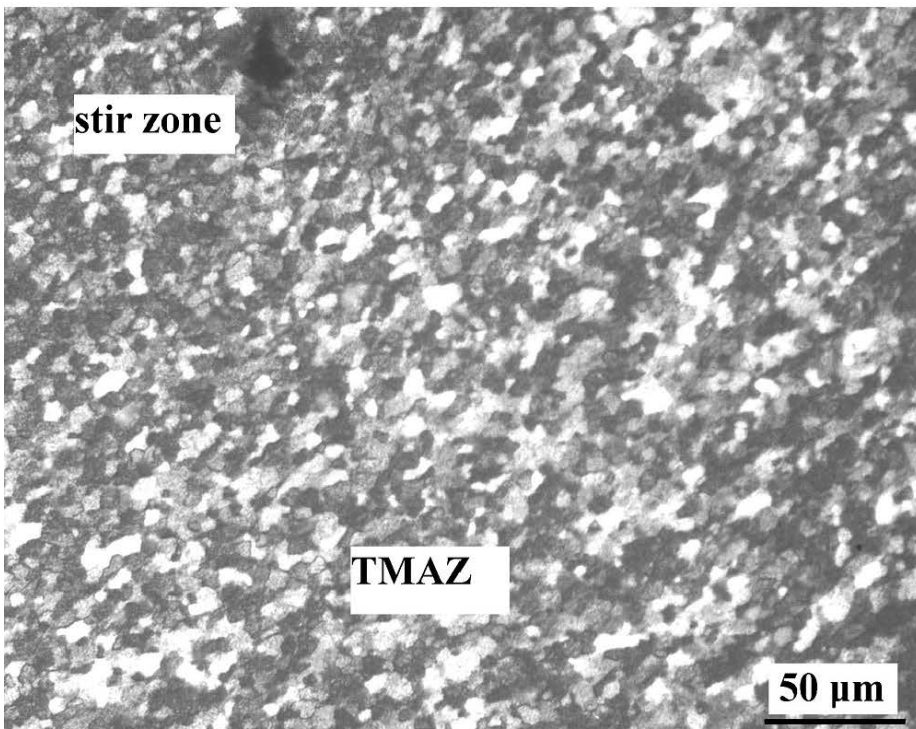
Figure 2 micro tensile specimen and test fixture



Figure 3 Macrostructure of a Friction stir welded joint in an Al 5083 alloy.



4 (a)



4 (b)

Figure 4 Microstructure of stir zone and TMAZ at the AS 4(a) and the RS 4(b)

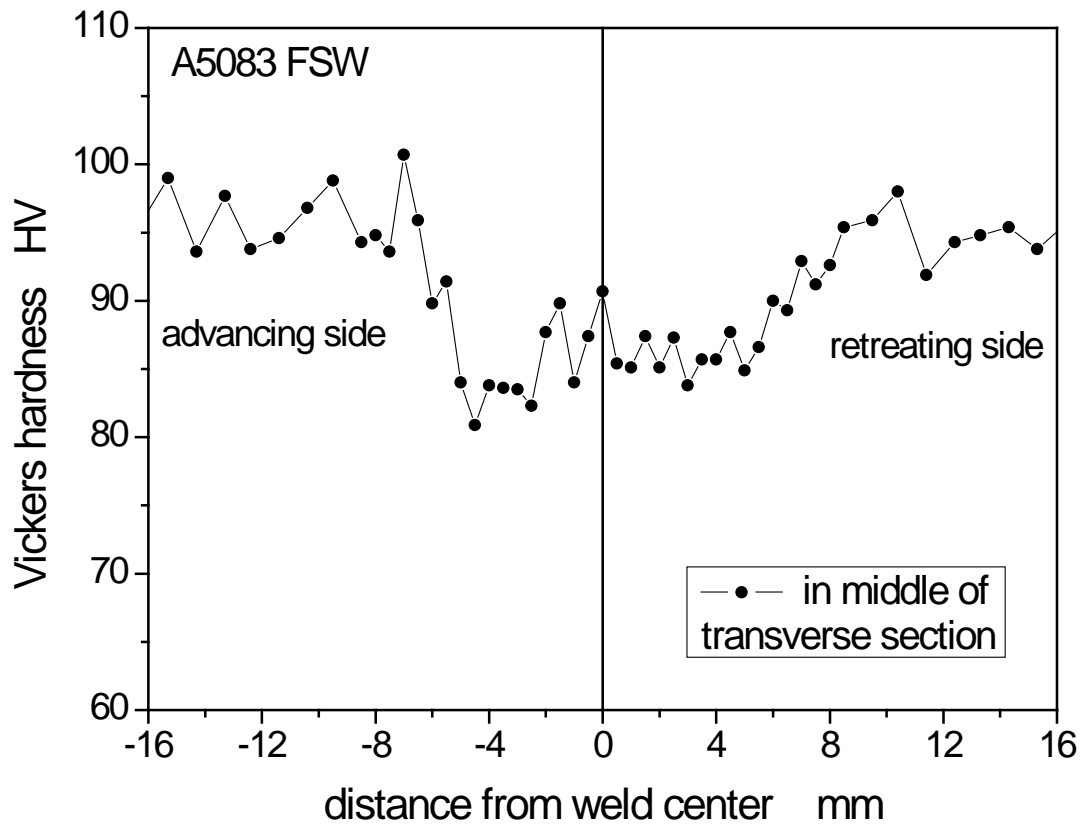


Figure 5 Hardness distribution on the weld joint.

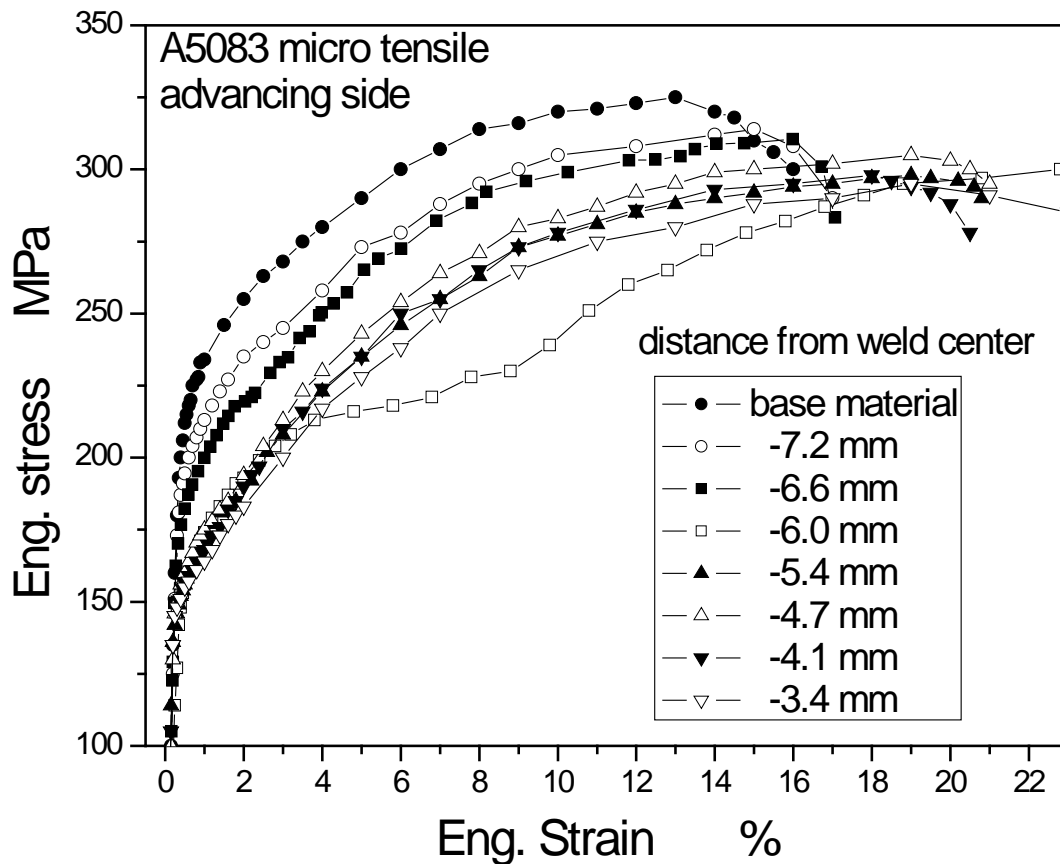


Figure 6 Engineering stress-strain curves at the AS of the FSW joint.

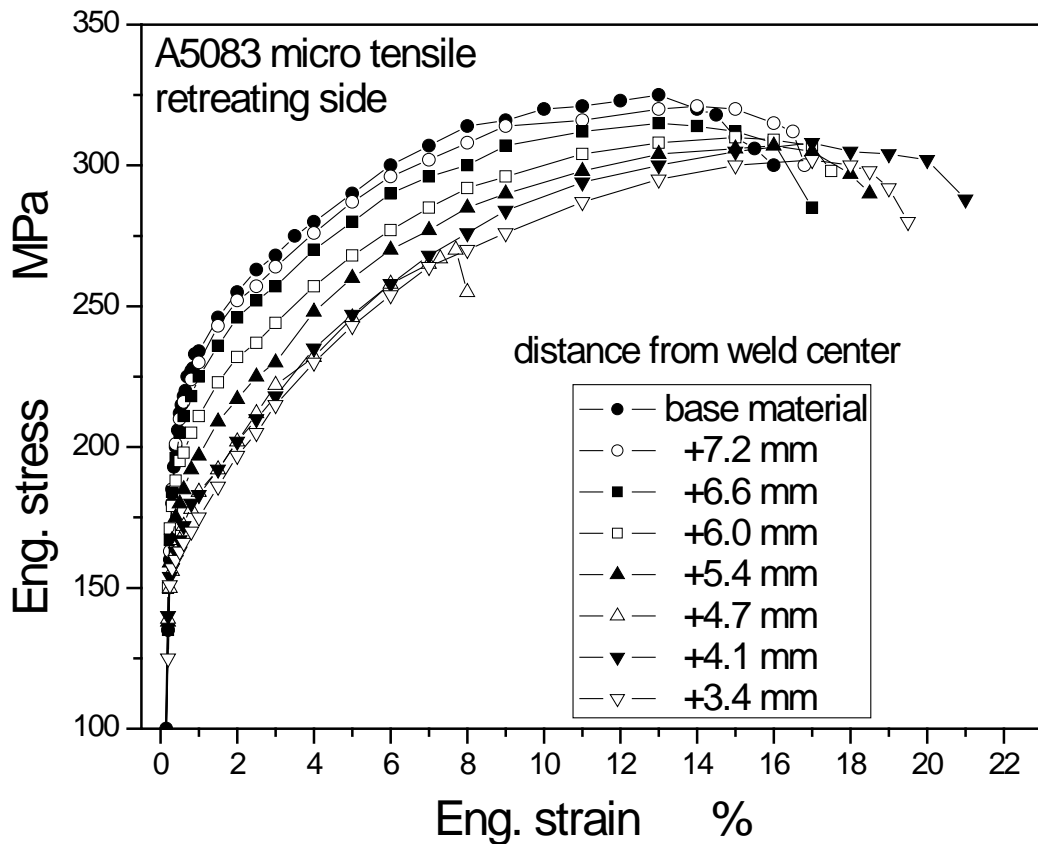


Figure 7 Engineering stress-strain curves at the RS of the FSW joint.

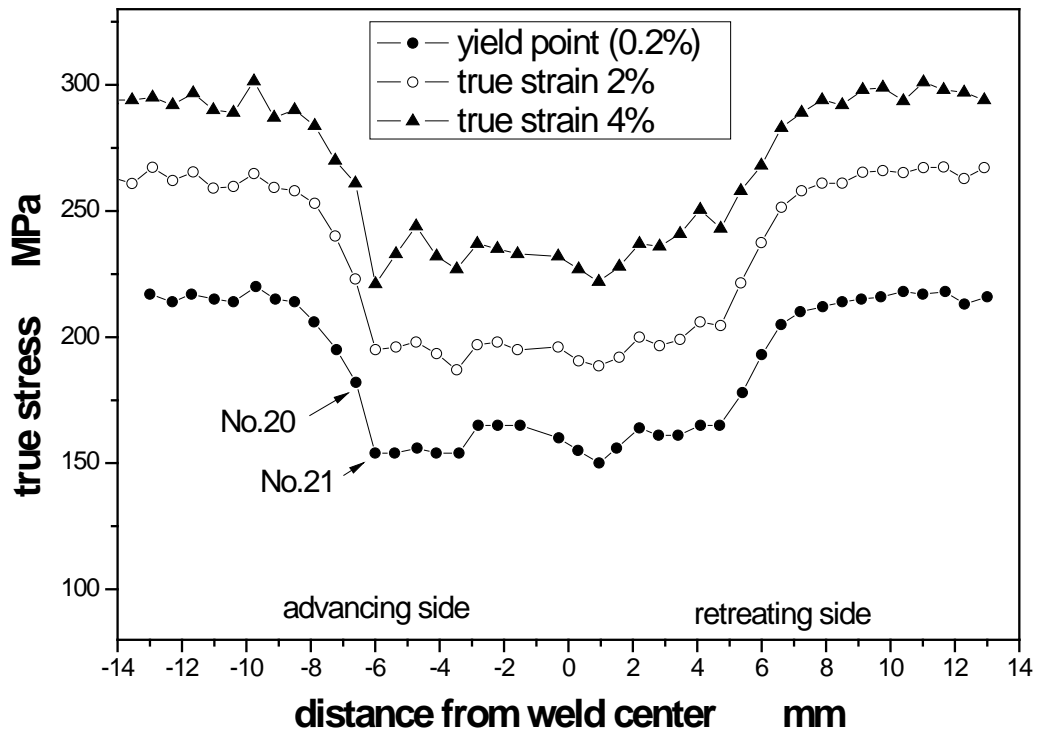


Figure 8 Tensile properties across the weld joint.

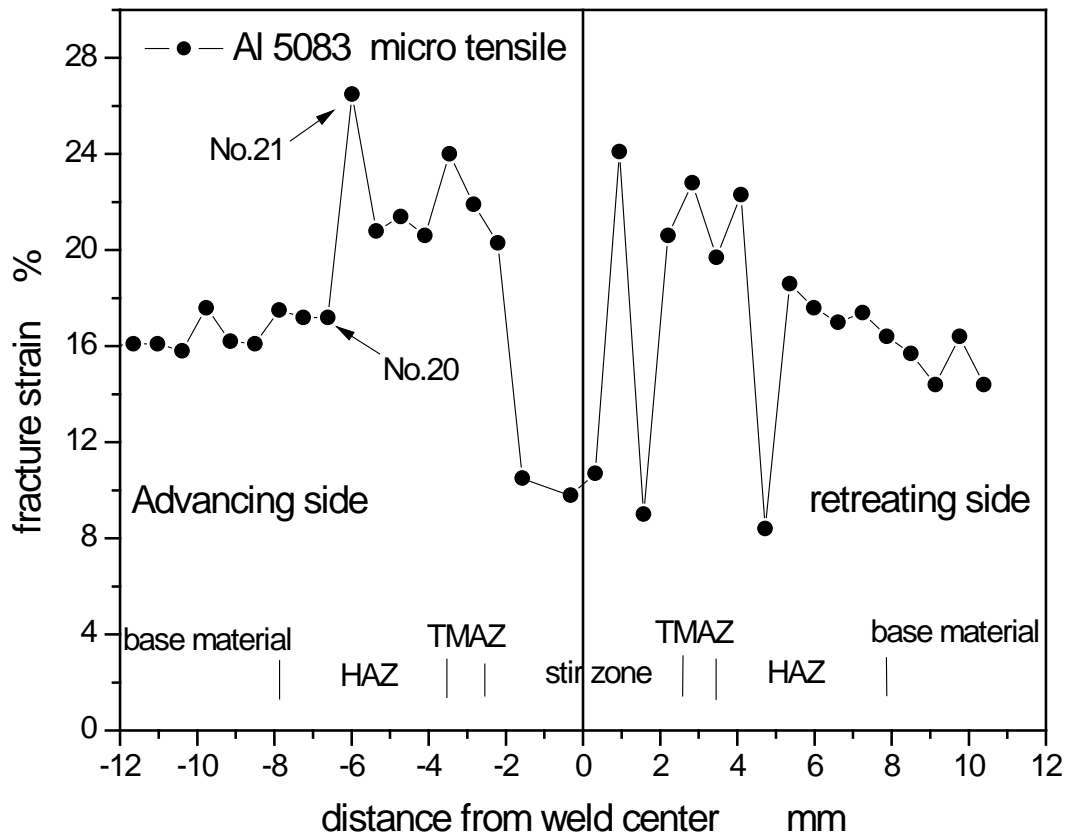


Figure 9 Fracture strain of micro-tensile specimens.

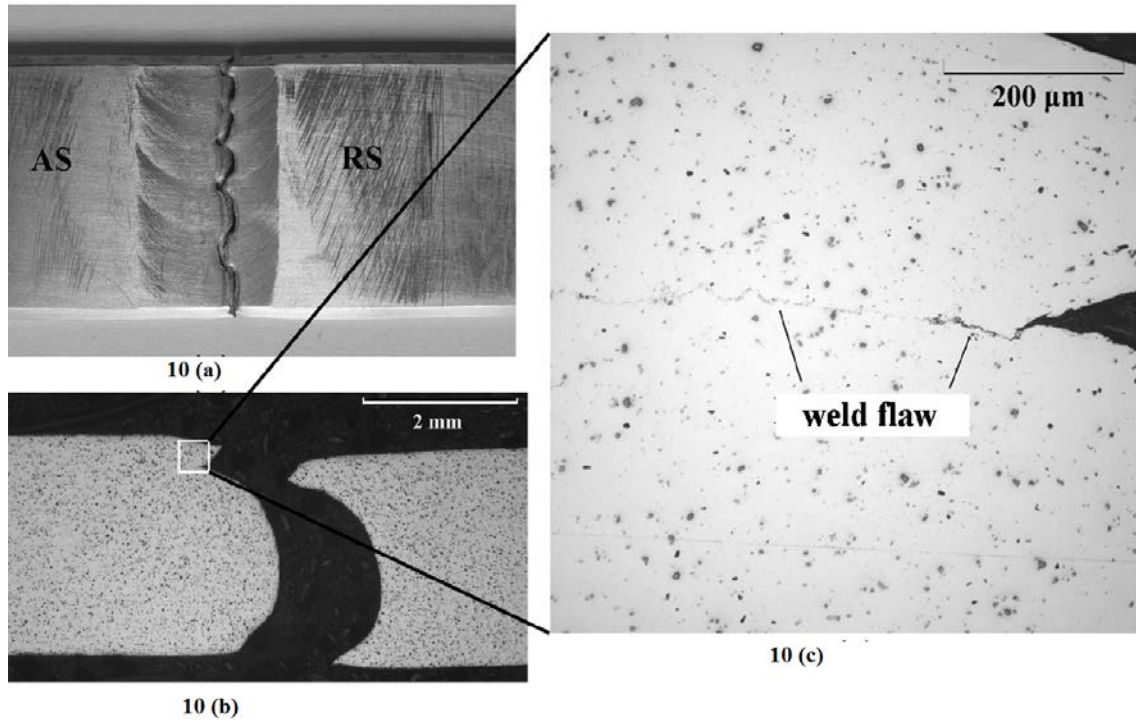


Figure 10 The fracture of a macro-tensile specimen: 10 (a) overview of fracture; 10 (b) cross section of fracture; 10 (c) a part of 10 (b) with weld flaw

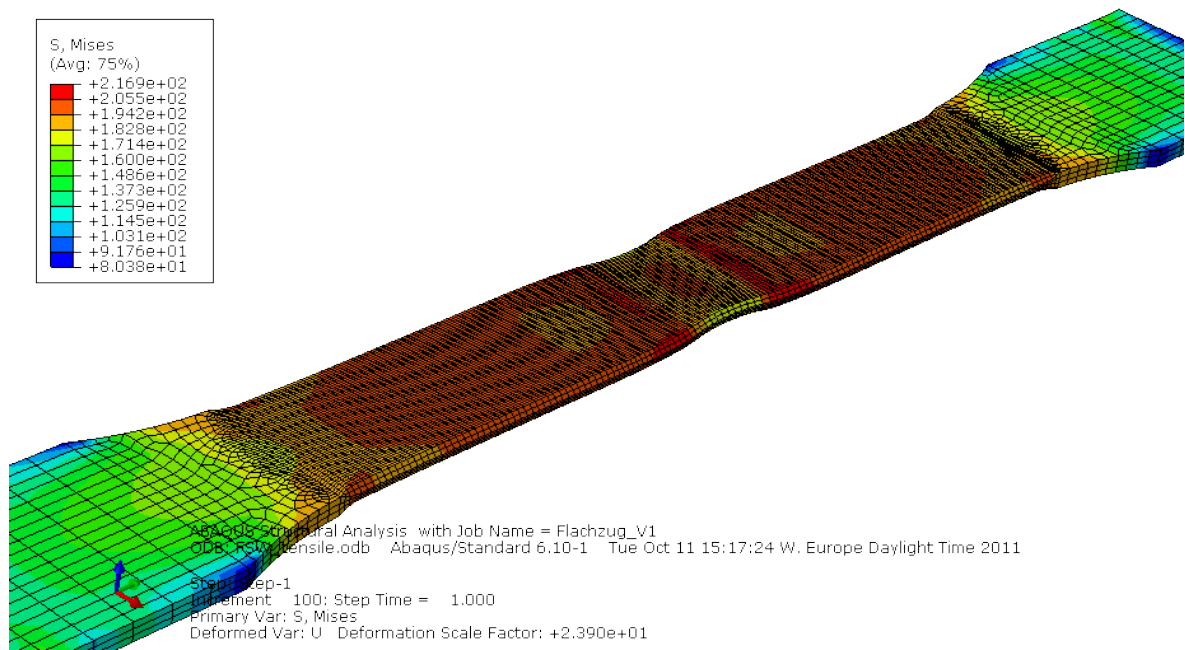


Figure 11 FEA examples of deformed macro tensile specimen

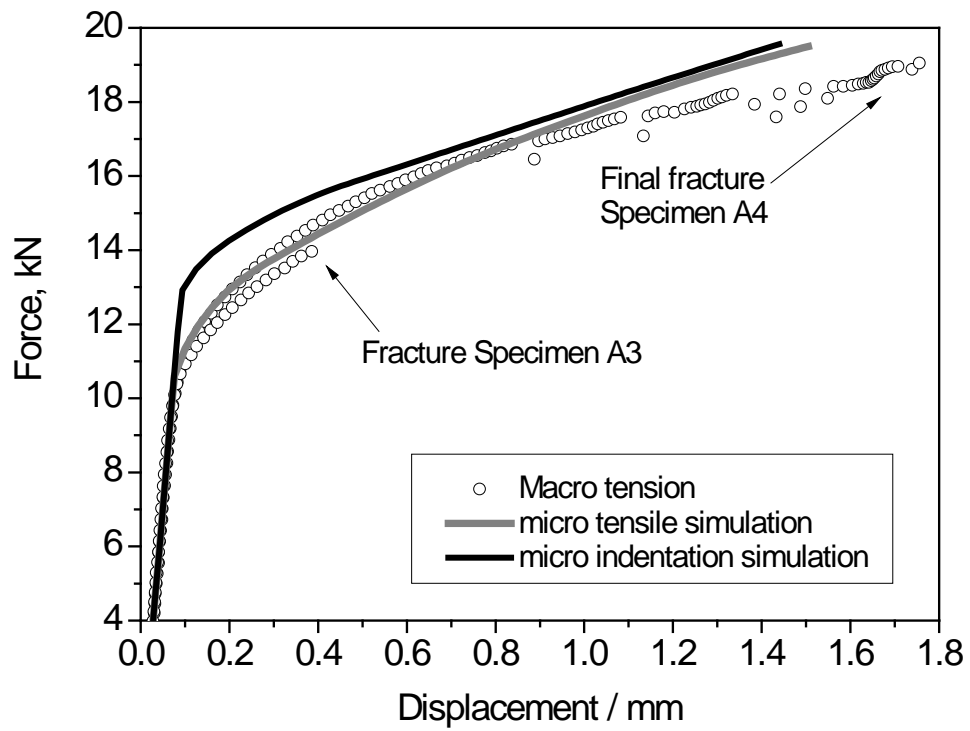


Figure 12 Comparison of macro tensile test data with Finite Element prediction results.